JACS
JOURNAL OF THE AMERICAN CHEMICAL SOCIETY

COMMUNICATION

pubs.acs.org/JACS

Water-Soluble Dual-Emitting Nanocrystals for Ratiometric Optical Thermometry

Emily J. McLaurin, Vladimir A. Vlaskin, and Daniel R. Gamelin*

Department of Chemistry, University of Washington, Box 351700, Seattle, Washington 98195-1700, United States

Supporting Information

ABSTRACT: Multishell semiconductor nanocrystals have been synthesized that display intrinsic dual emission with robust photo and thermal stability and attractive thermal sensitivity. Dual emission is demonstrated following phase transfer into aqueous media. These nanocrystals are suitable for diverse optical thermometric or thermographic applications in biotechnology or other areas.

Temperature plays critical roles in many biological and biotechnological processes ranging from calcium signaling[1] and protein folding[2] to polymerase chain reaction[3] and thermotherapy.[4] The importance of temperature in such processes has fueled interest in the development of *in situ* temperature sensors.[5,6] Measurement of the temperature-dependent photoluminescence (PL) intensities of molecular probes is a popular approach to thermometry in biotechnology.[7] This type of optical measurement is attractive because of its simplicity and excellent spatial and temporal resolution.[8] Numerous luminescent probes based on fluorescent dyes[7−10] and semiconductor nanocrystals[11−13] have been developed for this purpose.

Colloidal semiconductor nanocrystals (or quantum dots, QDs) are often used as fluorescent labels because of their photostabilities,[14] broad excitation profiles,[15] large absorption cross sections, and tunable emission energies.[16] The photophysical properties of QDs can be modified in a variety of ways, such as by heteroepitaxial shell growth, surface functionalization, or introduction of impurity ions (doping). Nanocrystals containing paramagnetic impurities are attractive as magnetic resonance imaging contrast agents.[17] In some cases, these impurities show efficient sensitized PL, making such materials also attractive for optical imaging[18] and sensing.[19]

We recently reported the discovery of a new photophysical process by which nanocrystals show intrinsic dual emission.[20] When Mn^{2+} ions were doped into wide-gap semiconductor nanocrystals such as ZnSe, photoexcitation of the semiconductor resulted in efficient sensitized Mn^{2+} luminescence (Figure 1A). However, when Mn^{2+} ions were doped into semiconductor nanocrystals with energy gaps above but close in energy to the lowest Mn^{2+} d−d excited state ($^4T_1$), for example $Zn_{1-x}Mn_xSe$/ZnCdSe core/shell nanocrystals, thermal equilibration of excited-state populations between the $^4T_1$ and excitonic states gave rise to two luminescence bands whose ratio was extremely sensitive to temperature (Figure 1B). The active dual-emission temperature windows could be tuned by adjusting the exciton−Mn^{2+}($^4T_1$) energy gap during nanocrystal synthesis.[20] Although a powerful proof of concept that allowed fundamental aspects of this dual-emission mechanism to be described in detail, the $Zn_{1-x}Mn_xSe$/ZnCdSe nanocrystals examined previously posed some practical limitations. A strong dependence of the nanocrystal energy gap on small numbers of surface Cd^{2+} ions made these structures susceptible to photo or thermal degradation over long experiment times, because loss of even a few Cd^{2+} ions changed the energy gap governing the thermal equilibrium. Such instabilities were exacerbated in aqueous media. The suitability of these

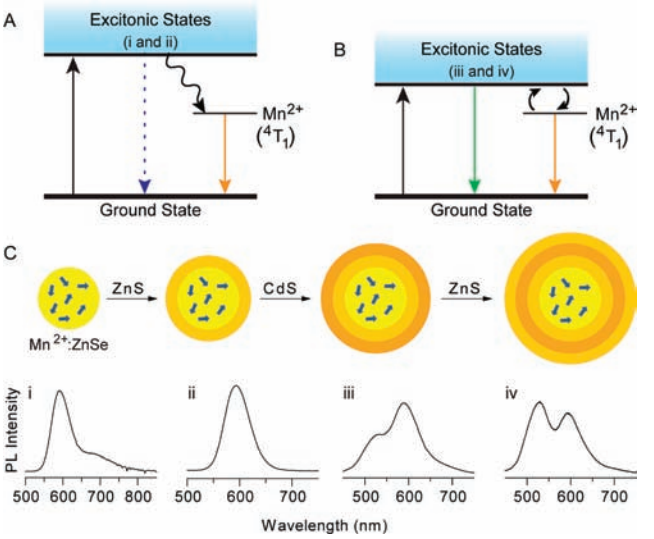

Figure 1. Dual-emitting Mn^{2+}-doped semiconductor nanocrystals. (A) Wide-gap Mn^{2+}-doped semiconductor nanocrystals such as $Zn_{1-x}Mn_xSe$ and $Zn_{1-x}Mn_xSe$/ZnS show efficient sensitized Mn^{2+} luminescence (orange arrow) following semiconductor photoexcitation (black arrow). (B) Narrowing the band gap allows thermal population of excitonic excited states by back energy transfer from Mn^{2+}($^4T_1$), yielding excitonic PL (green arrow) in addition to Mn^{2+} PL (orange arrow). (C) (*i*) Core $Zn_{1-x}Mn_xSe$ ($d \approx 3$ nm) nanocrystals show intense sensitized Mn^{2+} PL at ∼590 nm, as well as some trap PL at ∼700 nm. (*ii*) Growth of a ∼3 monolayer ZnS shell around these cores increases the Mn^{2+} PL QY while eliminating surface trap PL. (*iii*) Growth of a ∼1 monolayer CdS shell around the $Zn_{1-x}Mn_xSe$/ZnS nanocrystals narrows the energy gap and causes the appearance of excitonic PL at ∼525 nm, with a drop in PL QY. (*iv*) Growth of a final ∼3 monolayer ZnS shell around the $Zn_{1-x}Mn_xSe$/ZnS/CdS nanocrystals narrows the energy gap slightly, altering the relative intensities of the two PL features. The final nanocrystals have $d \approx 6$ nm and show intrinsic dual emission at room temperature with PL QYs up to ∼40%.

Received: July 25, 2011
Published: August 29, 2011

dx.doi.org/10.1021/ja206956t | *J. Am. Chem. Soc.* 2011, 133, 14978–14980

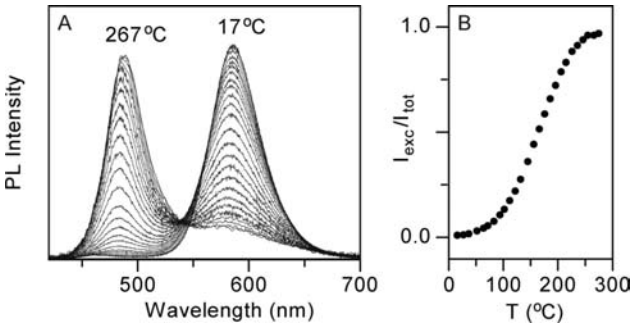

Figure 2. Thermal stability. (A) Variable-temperature PL spectra of colloidal $Zn_{1-x}Mn_xSe/ZnS/CdS/ZnS$ nanocrystals ($d \approx 7$ nm, 39% QY at room temperature, capped with TOPO), measured in octadecene under nitrogen. Spectra were normalized to total integrated intensity. (B) Thermometric response curve plotting I_{exc}/I_{tot} vs temperature for these nanocrystals. A maximum slope of 7.3×10^{-3} °C^{-1} was obtained.

nanocrystals for bio-related applications was also arguably compromised by the exposure of Cd^{2+} at their surfaces. Attempts to grow protective ZnS shells led to loss of the dual emission. We now report successful preparation of robust dual-emitting nanocrystals that are stable at high temperatures and in water, making them suitable for a broad range of applications including bioimaging.

Figure 1C summarizes the approach used in the present study to obtain stable, dual-emitting QDs. First, $Zn_{1-x}Mn_xSe$ cores (*i*) were prepared by previously reported methods.[21,22] These core nanocrystals were then coated with shells of ZnS (*ii*), CdS (*iii*), and ZnS again (*iv*), by adaptation of methods described previously.[23,24] Placement of Mn^{2+} in the QD cores ensures rapid exciton−Mn^{2+} energy transfer, and the initial ZnS shell layer significantly improves core PL quantum yields (QYs, typically from <∼10% to ∼40%), likely by passivation of surface trap states. For example, the trap-based PL near 700 nm is diminished upon ZnS shell growth. Growth of a CdS layer around the $Zn_{1-x}Mn_xSe/ZnS$ nanocrystals lowers the nanocrystal energy gap and results in appearance of excitonic PL to the blue of the Mn^{2+} PL (Figure 1C, *iii*). Beyond enhancing PL, the first ZnS shell serves as a buffer layer between the ZnSe core and the CdS layer, reducing the sensitivity of the bandgap energy to the addition of Cd^{2+} seen in our previous study by preventing formation of Cd−Se bonds. The ZnS buffer layer also reduces Mn^{2+} migration out of the ZnSe core, a problem encountered upon Cd^{2+} addition to $Zn_{1-x}Mn_xSe$ nanocrystals under some conditions. The final ZnS layer confines the exciton away from the surface, making the QDs more photostable.[25] Outer ZnS shells generally make QDs less prone to oxidation in aqueous solutions as well.[26] Overall, this multishell synthetic method allows more precise tuning of the bandgap, and hence of the dual emission, than was achieved previously. The product nanocrystals are brighter and more stable against degradation.

Figure 2 illustrates the robustness of the resulting dual-emitting nanocrystals. These nanocrystals exhibit exclusively Mn^{2+} emission (590 nm) at room temperature, with a PL QY of 39%. Upon heating, excitonic PL is observed at 510 nm, concomitant with a decrease of Mn^{2+} PL. At temperatures greater than ∼250 °C, the PL intensity has been shifted almost entirely from Mn^{2+} to the excitonic feature (Figure 2A). Figure 2B shows the thermometric response curve measured for these nanocrystals, plotting the ratio of the integrated excitonic emission (I_{exc}) to the total integrated

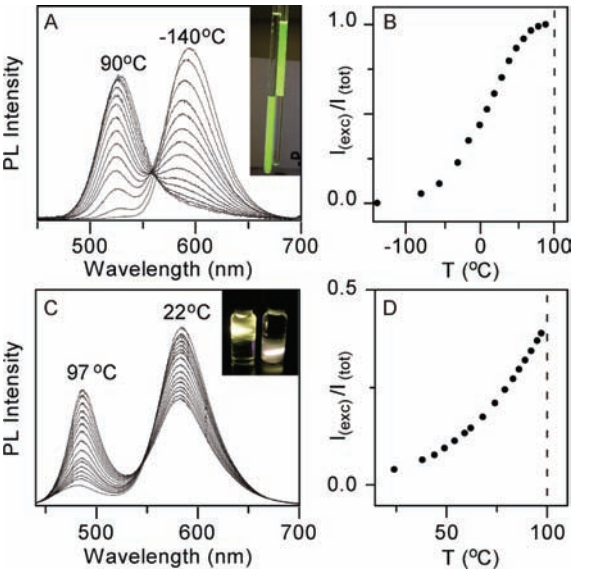

Figure 3. Water-soluble dual-emitting nanocrystals. (A) Variable-temperature PL spectra of citrate-capped $Zn_{1-x}Mn_xSe/ZnS/CdS/ZnS$ nanocrystals ($d \approx 5$ nm) in water. Spectra were normalized to the total integrated intensity. Inset: Photograph of the nanocrystals in water (left) and in toluene (right). The QY dropped from 15% to 10% upon phase transfer. (B) Thermometric response curve plotting I_{exc}/I_{tot} vs temperature for these nanocrystals. A maximum slope of 7.2×10^{-3} °C^{-1} was obtained. (C) Variable-temperature PL spectra of $Zn_{1-x}Mn_xSe/ZnS/CdS/ZnS$ nanocrystals encapsulated by *n*-octylamine-modified poly(acrylic acid), suspended in aqueous solution. The QY dropped from 24% to 19% upon phase transfer. Inset: Photograph of these nanocrystals in toluene (left) and in aqueous solution (right). (D) Thermometric response curve plotting I_{exc}/I_{tot} vs temperature for the polymer-encapsulated nanocrystals. A maximum slope of 8.3×10^{-3} °C^{-1} was obtained.

emission (I_{tot}) vs temperature. These data show a high thermometric sensitivity of $\sim 7 \times 10^{-3}$ °C^{-1} over a broad window of ∼100 °C. Their stability over extended measurement times at these high temperatures illustrates the thermal robustness of these core/multishell dual emitters.

For these nanocrystals to be useful in bioimaging, they must retain their dual emission in water. With robust dual-emitting nanocrystals in hand, expansion of this sensing scheme to aqueous environments was therefore pursued. It is well established that the photophysical properties of nanocrystals are highly dependent on their surfaces and the surrounding medium.[27−29] Our first-generation $Zn_{1-x}Mn_xSe/ZnCdSe$ dual emitters were unstable in water, likely due to Cd^{2+} loss from their surfaces. In contrast, the new multishell nanocrystals were found to be well suited for phase transfer.

Figure 3 demonstrates successful phase transfer of dual-emitting nanocrystals using two different methods. Exchange of the TOPO ligands with citrate[30] yielded nanocrystals exhibiting dual emission over the full temperature range of liquid water, from near its boiling point to well below its freezing point (Figure 3A). The photograph in the inset of Figure 3A shows these nanocrystals in toluene and in water. Their PL QY was 10% in water (decreased from 15%), and they showed no degradation over a period of days. Figure 3B plots the thermometric response curve measured for these nanocrystals in water, yielding a maximum sensitivity of 7.2×10^{-3} °C^{-1}. Noteworthy is the

continuity in this curve across the liquid−solid phase transition of water despite severe reduction in optical quality of the aqueous matrix. This result illustrates the powerful advantage of ratiometric optical thermometry.

Our best water solubilization was achieved using an encapsulating polymer that has the advantage of maintaining the native nanocrystal surface ligands even after phase transfer.[14] QDs prepared in this manner are stable for months or longer at room temperature. Figure 3C shows the temperature-dependent PL spectra of dual-emitting nanocrystals stabilized in water using *n*-octylamine-modified poly(acrylic acid). Predominantly Mn^{2+} emission is observed at room temperature, and excitonic emission increases upon sample heating. Figure 3D shows the thermometric response curve measured for these nanocrystals, which display a maximum sensitivity of 8.3×10^{-3} °C^{-1}.

In addition to sensitivity, important metrics for evaluation of ratiometric optical thermometers are the accuracy and precision with which they can report temperature. The accuracy of these probes is determined extrinsically when constructing the calibration curves. Reproducibility of these curves is excellent due to the stability of the nanocrystals, but their accuracy is only as good as the thermometers used during data collection. With a perfect calibration curve, the precision of the optical thermometers would be determined entirely by the signal-to-noise ratios of the PL spectra. For illustration, the ratio I_{exc}/I_{tot} can be determined from the data in Figure 3C,D with an error of $\pm 1.2 \times 10^{-3}$, which translates to a precision of ±0.14 °C over the entire data set. We note that this level of precision exceeds that of the thermometer used in collecting the data for the calibration curve (±0.5 °C). Each spectrum here was collected with 300 ms integration using a hand-held fiber spectrometer and no collection optics. Even higher precision can thus be obtained simply by extending integration times or improving the detection setup.

In summary, dual-emitting Mn^{2+}-doped semiconductor nanocrystals have been prepared that are stable at high temperatures and in water. Both of these advances expand the range of thermometric applications available for these sensors. In particular, with stability of these dual emitters now demonstrated in aqueous environments, the door is opened for biological or biotechnological applications, for example thermographic imaging of microfluidic PCR devices or thermometric analysis of fundamental biological processes such as cell death or protein denaturation.

■ ASSOCIATED CONTENT

Ⓢ Supporting Information. Detailed descriptions of syntheses, measurements, and additional results. This material is available free of charge via the Internet at http://pubs.acs.org.

■ AUTHOR INFORMATION

Corresponding Author
Gamelin@chem.washington.edu

■ ACKNOWLEDGMENT

The authors thank the Washington Research Foundation for generous support of this research. Financial support from the US NSF (DMR-0906814) and the University of Washington is also gratefully acknowledged. Part of this work was conducted at the University of Washington NanoTech User Facility, a member of the NSF National Nanotechnology Infrastructure Network. We also thank Mr. Liam Bradshaw for helpful discussions and experimental assistance.

■ REFERENCES

(1) Clausen, T.; Vanhardeveld, C.; Everts, M. E. *Physiol. Rev.* **1991**, *71*, 733.
(2) Murphy, K. P.; Freire, E. *Adv. Protein Chem.* **1992**, *43*, 313.
(3) Zhang, C. S.; Xing, D. *Nucleic Acids Res.* **2007**, *35*, 4223.
(4) Sapareto, S. A.; Dewey, W. C. *Int. J. Radiat. Oncol. Biol. Phys.* **1984**, *10*, 787.
(5) Gosse, C.; Bergaud, C.; Low, P. Molecular Probes for Thermometry in Microfluidic Devices. In *Thermal Nanosystems and Nanomaterials*; Volz, S., Ed.; Topics in Applied Physics 118; Springer-Verlag: Berlin, 2009; p 301.
(6) McCabe, K. M.; Hernandez, M. *Pediatr. Res.* **2010**, *67*, 469.
(7) Uchiyama, S.; de Silva, A. P.; Iwai, K. *J. Chem. Educ.* **2006**, *83*, 720.
(8) Ross, D.; Gaitan, M.; Locascio, L. E. *Anal. Chem.* **2001**, *73*, 4117.
(9) Lou, J. F.; Hatton, T. A.; Laibinis, P. E. *Anal. Chem.* **1997**, *69*, 1262.
(10) Schrum, K. F.; Williams, A. M.; Haerther, S. A.; Benamotz, D. *Anal. Chem.* **1994**, *66*, 2788.
(11) Wang, S. P.; Westcott, S.; Chen, W. *J. Phys. Chem. B* **2002**, *106*, 11203.
(12) Walker, G.; Sundar, V.; Rudzinski, C.; Wun, A.; Bawendi, M.; Nocera, D. *App. Phys. Lett.* **2003**, *83*, 3555.
(13) Han, B.; Hanson, W. L.; Bensalah, K.; Tuncel, A.; Stern, J. M.; Cadeddu, J. A. *Ann. Biomed. Eng.* **2009**, *37*, 1230.
(14) Wu, X. Y.; Liu, H. J.; Liu, J. Q.; Haley, K. N.; Treadway, J. A.; Larson, J. P.; Ge, N. F.; Peale, F.; Bruchez, M. P. *Nat. Biotechnol.* **2003**, *21*, 41.
(15) Murray, C. B.; Norris, D. J.; Bawendi, M. G. *J. Am. Chem. Soc.* **1993**, *115*, 8706.
(16) Chan, W. C. W.; Maxwell, D. J.; Gao, X. H.; Bailey, R. E.; Han, M. Y.; Nie, S. M. *Curr. Opin. Biotechnol.* **2002**, *13*, 40.
(17) Mornet, S.; Vasseur, S.; Grasset, F.; Duguet, E. *J. Mater. Chem.* **2004**, *14*, 2161.
(18) Louie, A. *Chem. Rev.* **2010**, *110*, 3146.
(19) Thakar, R.; Chen, Y. C.; Snee, P. T. *Nano Lett.* **2007**, *7*, 3429.
(20) Vlaskin, V. A.; Janssen, N.; van Rijssel, J.; Beaulac, R.; Gamelin, D. R. *Nano Lett.* **2010**, *10*, 3670.
(21) Archer, P. I.; Santangelo, S. A.; Gamelin, D. R. *J. Am. Chem. Soc.* **2007**, *129*, 9808.
(22) Archer, P. I.; Santangelo, S. A.; Gamelin, D. R. *Nano Lett.* **2007**, *7*, 1037.
(23) Li, J. J.; Wang, Y. A.; Guo, W.; Keay, J. C.; Mishima, T. D.; Johnson, M. B.; Peng, X. *J. Am. Chem. Soc.* **2003**, *125*, 12567.
(24) Chen, H.-S.; Lo, B.; Hwang, J.-Y.; Chang, G.-Y.; Chen, C.-M.; Tasi, S.-J.; Wang, S.-J. J. *J. Phys. Chem. B* **2004**, *108*, 17119.
(25) Reiss, P.; Protiere, M.; Li, L. *Small* **2009**, *5*, 154.
(26) Medintz, I. L.; Uyeda, H. T.; Goldman, E. R.; Mattoussi, H. *Nat. Mater.* **2005**, *4*, 435.
(27) Nose, K.; Fujita, H.; Omata, T.; Otsuka-Yao-Matsuo, S.; Nakamura, H.; Maeda, H. *J. Lumin.* **2007**, *126*, 21.
(28) Pilla, V.; Alves, L. P.; Munin, E.; Pacheco, M. T. T. *Opt. Commun.* **2007**, *280*, 225.
(29) Munro, A. M.; Jen-La Plante, I.; Ng, M. S.; Ginger, D. S. *J. Phys. Chem. C* **2007**, *111*, 6220.
(30) Rogach, A. L.; Nagesha, D.; Ostrander, J. W.; Giersig, M.; Kotov, N. A. *Chem. Mater.* **2000**, *12*, 2676.